Efficient procedure for the measurement of preresonant excitation profiles in UV Raman spectroscopy

Martin Höhl, Bernhard Roth, Uwe Morgner, and Merve Meinhardt-Wollweber

Citation: Review of Scientific Instruments **88**, 073105 (2017);
View online: https://doi.org/10.1063/1.4994891
View Table of Contents: http://aip.scitation.org/toc/rsi/88/7
Published by the American Institute of Physics

Efficient procedure for the measurement of preresonant excitation profiles in UV Raman spectroscopy

Martin Höhl,[1,2,a),b)] Bernhard Roth,[2] Uwe Morgner,[1,2,b)] and Merve Meinhardt-Wollweber[1,2,b)]
[1]*Institut für Quantenoptik, Leibniz Universität Hannover, Hannover 30167, Germany*
[2]*Hannoversches Zentrum für Optische Technologien, Leibniz Universität Hannover, Hannover 30167, Germany*

(Received 26 October 2016; accepted 7 July 2017; published online 25 July 2017)

Resonance Raman spectroscopy (RRS) is a promising technique for investigating samples with low concentrations of single constituents or many different constituents. The wavelength dependent resonance enhancement (resonance profile) of the respective molecule yields information about the targeted species and reveals the optimal wavelength for high resolution RRS. A significant increase of the Raman scattered intensity can already be achieved in the vicinity of the molecules' absorption band (preresonance). Measuring such preresonance and resonance profiles requires precise control of excitation conditions and careful assessment of the spectral accuracy of the setup. We present a comprehensive procedure for the acquisition of preresonance profiles in Raman spectroscopy. An experimental setup for recording the single spectra is combined with an efficient algorithm for data postprocessing. The procedure is demonstrated on amino acids measured in the UV and can be applied to any molecule and wavelength range. *Published by AIP Publishing.* [http://dx.doi.org/10.1063/1.4994891]

I. INTRODUCTION

Raman spectroscopy is a versatile tool for investigating the properties of molecules in a nondestructive manner. The accessible information ranges from identification of constituents and their concentration,[1] characterization (e.g., drug binding or adsorption of molecules on surfaces),[2,3] and molecular structure[4–6] to folding of molecules[7] and protein channel gating mechanisms.[8] Obtaining this information requires a highly sensitive experimental setup in terms of spectral resolution and detection efficiency, as the cross section of Raman scattering is small compared to that of light absorption or fluorescence.[9] Several techniques are used regularly to increase the sensitivity in Raman spectroscopy. For example, surface enhanced Raman spectroscopy (SERS) and tip enhanced Raman spectroscopy (TERS) are applied. They benefit from electromagnetic field enhancement from local surface plasmon polaritons of metal nanoparticles. Chemical enhancement mechanisms connected with charge transfer to the attached Raman active target molecules are also involved. However, performing *in vivo* measurements excludes techniques like SERS or TERS, usually requiring an extensive sample preparation. In contrast, resonance Raman spectroscopy (RRS) utilizes electronic resonances of the Raman active molecules, resulting in a larger scattering cross section as compared to normal Raman scattering. A significant increase in the Raman scattered light can be observed when approaching a molecular absorption band.[10,11] Maximal enhancement is achieved at or close to specific absorption bands (resonance) but also excitation at the wings of these absorption peaks leads to significant signal enhancement (preresonance). Since each molecule has a unique absorption spectrum, the appropriate excitation wavelengths used for RRS are also specific to the molecule. A majority of biomolecules (e.g., proteins) are studied in the ultraviolet (UV) and the visible range. The absorption maxima of small molecules, such as amino acids, are typically in the deep UV range.[12,13]

The implementation of high resolution RRS does not require significant changes in the experimental setup for normal Raman spectroscopy. However, the excitation wavelength best fitting the analyte needs to be determined beforehand. For this purpose, the wavelength dependent resonance enhancement (resonance profile) of the analyte needs to be recorded, necessitating a broad range of excitation wavelengths and a spectrograph calibrated for the whole range. The latter is difficult to achieve in the UV due to the limited availability of calibrated light sources. As a consequence, published data about the resonant enhancement of (small) biomolecules (especially in the UV) are sparse.[4,6,14–24] All of the published studies were performed at discrete wavelengths. By using a continuous range of excitation wavelengths, it is possible to scan for sharp resonances. Recording the resonance profile of a specific molecule or investigating different molecules in one sample with the same setup significantly increases the demands on instrumentation, spectral characterization of the setup, and experimental parameters. Furthermore, consistent excitation conditions (e.g., same accumulated energy irradiated in the sample for each excitation wavelength) are required.

In contrast to normal Raman spectroscopy, where spectra are routinely vector-normalized for better comparability, the absolute and relative Raman intensity is an important parameter in RRS. This requires the monitoring of the energy applied to the sample to correct for variations of the Raman intensity due to power fluctuations of the light source. A broad excitation range normally requires shifting the limited

a)Electronic mail: martin.hoehl@hot.uni-hannover.de
b)See www.hearing4all.eu for information on Cluster of Excellence "Hearing4all."

spectral detection range, for example, by moving the grating of the spectrograph, demanding a more extensive calibration. Moreover, a complete characterization of the spectral sensitivity of the system is essential for recording Raman resonance profiles. For this purpose, the device spectral response function (DSRF) needs to be recorded.

Consequently, the requirements for measuring high resolution resonance profiles of molecules are a broadly tunable narrowband light source, a device for tracking the energy applied to the samples, compatible spectral filters for blocking Rayleigh scattered light at each excitation wavelength, a spectrograph with a broad spectral acquisition range, and an efficient procedure for postprocessing the recorded spectra. The postprocessing requires an effective background correction for the individual spectra and needs to account for the wavelength dependent response of the experimental setup.

Here we present a technique to measure resonance profiles of amino acids in aqueous solutions in the range from 244.8 nm to 266.0 nm with a resolution of 0.1 nm by using an optical parametric oscillator (OPO) as the light source and an algorithm for postprocessing the recorded Raman spectra. The technique can be applied to any molecule and wavelength for obtaining the optimal wavelength to record the Raman spectrum of that molecule and to map resonance profiles in a broad and continuous range. Furthermore, the calibration procedure is able to correct spectral regions where there are no suitable calibration light sources available.

II. METHOD AND MATERIALS

A. Experimental

The experimental setup is depicted in Fig. 1. An optical parametric oscillator (OPO, Ekspla PG122/UV) is used for excitation. The UV light is generated by frequency doubling the signal wavelength leaving the OPO cavity and is tunable in 0.1 nm steps between 210.0 nm and 354.0 nm. The repetition rate of the pump laser is 10 Hz. Unconverted light is removed by a dichroic mirror (D, Semrock SEM-FF347-Di01-25x36). A telescope (L1 and L2) is used for beam shaping. The energy applied with each laser pulse is monitored by reflecting a small portion of the beam onto a photodiode (PD, Thorlabs DET10A/M) using a fused silica plate (B). The signal of the photodiode was calibrated using a calibrated pyroelectric energy sensor (Thorlabs ES111C). The light used for exciting the Raman spectra is focused into a cuvette (C) holding the sample. The cuvette is made of fused silica and has a light path of 10 mm. The mean energy of the pulses used for the excitation of Raman spectra was in the range of 0.28 mJ to 1.18 mJ. Together with the repetition rate of the laser (10 Hz), this results in an average power of less than 12 mW. The scattered light is guided through a long pass filter blocking the Rayleigh scattered light (LP, Semrock SEM-LP02-248RS-25, SEM-LP02-257RU-25, or SEM-LP02-266RU-25, depending on the excitation wavelength used). The Raman scattered light is focused (L5) into a step index fiber (F, Thorlabs UM22-100, core diameter of 100 μm) guiding it to a spectrograph (Andor Shamrock SR-500i-C-R with an Andor Newton DU940P-BU camera) for detection. The spectrograph is equipped with a grating in reflection mode having 2400 lines per millimeter blazed for 300 nm. In order to detect all Raman spectra, this grating is turned by a motorized stage according to the excitation wavelength. A minimal number of three grating positions cover the intended excitation range of 244.8 nm to 266.0 nm. The grating position used for the shortest excitation wavelength maps over 3000 wavenumbers onto the detector. The end facet of the fiber acts as the entrance slit of the spectrograph. A spectral resolution of 12 cm^{-1} for the Raman spectra was achieved. This value was obtained by fitting the spectra of Rayleigh scattered light via a Voigt profile and the long pass filters removed.

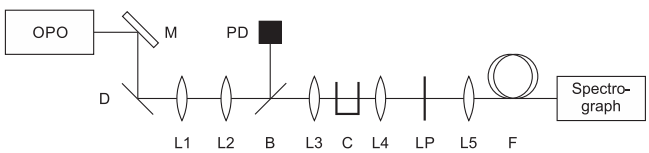

FIG. 1. Schematic of the experimental setup. OPO: optical parametric oscillator, M: mirror (aluminum), D: dichroic mirror, L1: f = 75 mm lens, L2: f = 30 mm lens, B: beam splitter, PD: photodiode, L3: f = 20 mm lens, C: cuvette, L4: f = 20 mm lens, LP: long pass filter, L5: f = 50 mm lens, F: fiber.

B. Excitation-emission map

The dependence of the Raman intensity on the excitation wavelength is visualized in an excitation-emission map (EEM) showing the relation between the Raman intensity and excitation wavelength. The measurement of high resolution resonance profiles over a wide range requires spectra excited at many different wavelengths. In an EEM, the individual Raman spectra need to be comparable in terms of Raman shift and intensity; therefore, reproducible and defined measurement conditions are crucial. Hence, in this work, we use the same light source for acquisition of the Raman spectra and for calibration of the experimental setup.

The accessible excitation range for an EEM not only depends on the light source but also on the possibility to block the excitation wavelength in the detection path, i.e., the availability of notch or long pass filters. The Raman filters integrated in the setup have an edge wavelength of 251.1 nm, 259.2 nm, and 268.6 nm, respectively, an edge steepness below 320 cm^{-1}, and a transmission of over 90% beyond the edge. The filters are normally optimized for one single wavelength. However, for the experiments presented here, the Raman filters were used for a range of excitation wavelengths. To do so, the long wavelength limit was selected to keep the remaining Rayleigh scattered light on the same intensity level as the Raman intensity. The short wavelength limit was chosen to cover at least half of the fingerprint region with the transmission range of the filter. The fingerprint region holding the characteristic Raman features of most biomolecules ranges from 500 cm^{-1} to 1700 cm^{-1} and covers only a small part of the spectral detection region of the camera. As stated above, filters designed for excitation at 248 nm, 257 nm, and 266 nm were used, leading to three excitation regions: region I ranges from 244.8 nm to 249.7 nm, II from 252.4 nm to 257.6 nm, and III from 260.3 nm to 266.0 nm, respectively. Since these

regions do not overlap, the EEM is not continuous but divided into three parts. As these regions are fairly narrow, a change of the grating position was not required for measurements within each region.

C. Calibration

An energy calibration of the photodiode was performed to account for the wavelength dependent energy output of the OPO. Fifty pulses of each excitation wavelength were emitted and simultaneously detected by the photodiode and the pyroelectric sensor. A linear regression model was applied to obtain the response function of the photodiode. In total, 323 different wavelengths in the range from 244.8 nm to 278.7 nm were included for acquiring the DSRF and the EEMs. The response function of the photodiode as well as the mean energy per pulse for each wavelength was derived from the data obtained for calibration. The mean energy per pulse and wavelength is required for applying the same amount of energy to the sample at each wavelength. An energy of 250 mJ was applied to each sample during this study.

The device spectral response function (DSRF) is used to correct the Raman spectra in terms of Raman spectral intensities to compensate for the wavelength dependent sensitivity of the setup. It needs to be determined individually for any setup and be applied to the Raman intensity spectra during postprocessing.

In order to determine the DSRF, a cuvette with distilled water served as base reference. Since the transmitted laser signal amplitude was used to measure the spectral response of the setup, these measurements were performed in the transmission bands of the Raman filters. A neutral density filter (Thorlabs NDUV40A) was placed between the fourth lens (L4) and the long pass filter (LP, compare Fig. 1) to prevent saturation of the camera. In total, there were three sets of excitation wavelengths merged in the DSRF, one for each combination of filter and grating position. Overlapping parts were measured twice due to the change in the diffraction efficiency for each grating position. Every section of the DSRF corresponds to one particular set of excitation wavelengths, irrespective of any overlap. The following procedure is used to obtain the DSRF of the experimental setup. One pulse per wavelength was emitted by the OPO and the spectrum of this pulse was recorded with an exposure time of 1 s. A regression of that spectrum with a Voigt profile was performed to obtain the peak height directly from the fit parameters as a figure of merit. Values below 1.5 times the background level (stated by the mean of the spectrum) and values saturating the detector were excluded. If not otherwise stated, only regressions exceeding a quality factor (adjusted R^2) of 0.95 were taken into account. The peak height was divided by the energy measured by the calibrated photodiode to take fluctuations of the pulse energy into account. This procedure was repeated five times to obtain the averaged DSRF depicted in Fig. 2. The plot was smoothed by a moving average filter function with a span size of 2 nm to establish a continuous response function.

In data postprocessing, the spectral Raman intensity will be divided by the DSRF. Consequently, the spectral amplitudes of all data in Sec. III B were corrected via this spectral response characteristic for the setup shown in Fig. 1.

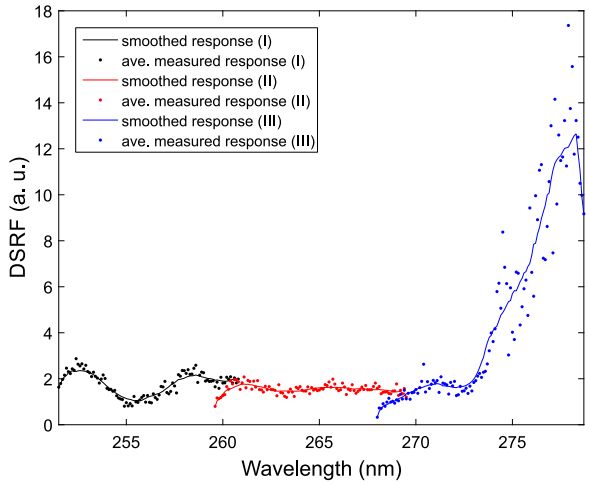

FIG. 2. Device spectral response function (DSRF) of the experimental setup as measured using a water reference sample. Points show the average value from five measurements at the respective wavelength. The smoothed continuous function (solid line) is derived from these points. This DSRF is used for the sensitivity correction of the spectra (black curve belongs to the excitation region I, and red and blue curves belong to regions II and III, respectively).

The finite reproducibility of the turret position for the movable grating in the spectrograph causes an offset of up to 105 wavenumbers. The offset was determined by removing the Raman filters from the setup and following the procedure for obtaining the DSRF. The position of the Rayleigh peak is used to shift the origin of the relative wavenumber axis to that position.

D. Sample preparation

In this work, the recording of resonance profiles is exemplarily demonstrated for proline and glycine. These molecules exhibit the highest solubility of all proteinogenic amino acids in water (c_{max} = 14.1M for proline and c_{max} = 3.3M for glycine[25]); thus, a high Raman intensity can be generated at a short exposure time. Here aqueous solutions of proline (Sigma-Aldrich 81709-25G) and glycine (Sigma-Aldrich G7126-100G) with a concentration c = 2.8M each were prepared for the EEM measurements. UV Raman spectroscopic studies of samples with a high concentration are affected by self-absorption and photodecomposition/photodegradation effects. However, these issues are beyond the scope of this work. The correction of specific Raman cross sections of distinct bonds due to self-absorption is described elsewhere.[22–24] The photodecomposition/photodegradation effects can be minimized by recirculating the sample in a capillary or through an open-air jet nozzle.[26]

For comparing the absorption of amino acids with the resonant enhancement in RRS, the absorption profiles of proline and glycine were measured. Aqueous solutions of these molecules were filled in cuvettes and placed inside a spectrophotometer (Kontron Instruments Uvikon 931) using a cuvette with distilled water for reference. All samples were analyzed directly after their preparation to minimize a

possible influence of dipeptides or larger molecules formed in the solution.

III. RESULTS AND DISCUSSION

A. Absorption and excitation range

The measured absorption spectra of proline and glycine are shown in Fig. 3. The absorption profiles of the amino acids recorded in this work and the excitation range applied are illustrated in Fig. 3(a). For these measurements, the samples were diluted (independently from each other) to stay within the optimal parameters of the spectrophotometer. The absolute absorption of proline and glycine is thus not comparable in Fig. 3(a). To have a closer look at the absorption profiles in the excitation range, undiluted samples (like those used for Raman measurements) are shown for comparison [proline c = 3.0M and glycine c = 2.4M, see Fig. 3(b)]. These concentrations differ from the ones used for the acquisition of resonance profiles since these measurements were performed at another date and fresh samples are required to exclude any sample degradation. The normalization of the results incorporates different sample concentrations.

The absorption spectra of proline and glycine show a significant increase in absorption towards shorter wavelengths starting at approximately 240 nm [Fig. 3(a)], whereas the increase in absorption within the excitation range indicates that the amino acids can be preresonantly excited [Fig. 3(b)].

B. Data postprocessing

For obtaining an EEM, different steps of data postprocessing are required. In Fig. 4, the flow chart for data processing is shown.

In step (1), the Raman spectra are shifted by the calculated offset of each excitation wavelength. In step (2), artifacts caused by cosmic rays are removed from the raw spectra by comparing the intensity of each data point with the intensities of the two adjacent points. If both differences exceed a threshold, the processed data point is replaced by the mean of the two adjacent data points. The threshold is selected not to alter any Raman intensities and set to ten times the mean of all intensity differences of adjacent data points. This algorithm reviews all intensities automatically. Depending on the excitation wavelength, the measurement of Raman spectra may include a fluorescent background. For excitation wavelengths below 250 nm, the fluorescence is usually located outside the region of interest.[27] Most of the excitation wavelengths applied in this work are larger than 250 nm, making a background correction necessary. Moreover, the procedure presented here also works for the application of visible excitation wavelengths, where the issue of fluorescence is important. The measurement of Raman spectra in the preresonant region usually also includes a fluorescent background. In step (3), the iterative morphological and mollifier-based baseline correction algorithm developed by Koch *et al.* was applied.[28] All spectra were corrected with the same set of parameters. In step (4), the DSRF for each spectral region (as defined by the filters) is used to correct the spectra with respect to the varying optical properties of the setup. In the fifth (and last) step (5), each spectrum is multiplied by the ratio of the actual to the shortest excitation wavelength used in the experiment to the power of four to account for the strong wavelength dependence ($\sim\lambda^{-4}$) of the scattering cross section. Thereby, the development of the resonance profiles is restricted on the resonance enhancement only. In addition, all spectra were divided by the energy

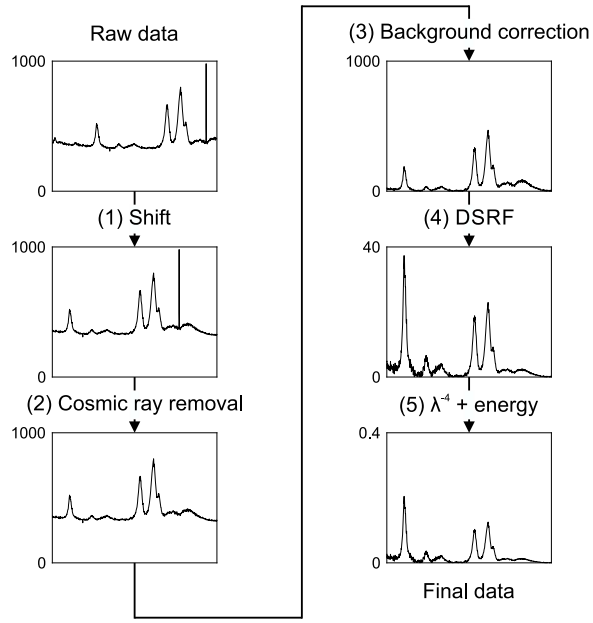

FIG. 4. Flow chart for data postprocessing. This sequence revises all spectra for comparison and enables the generation of an excitation-emission map (EEM).

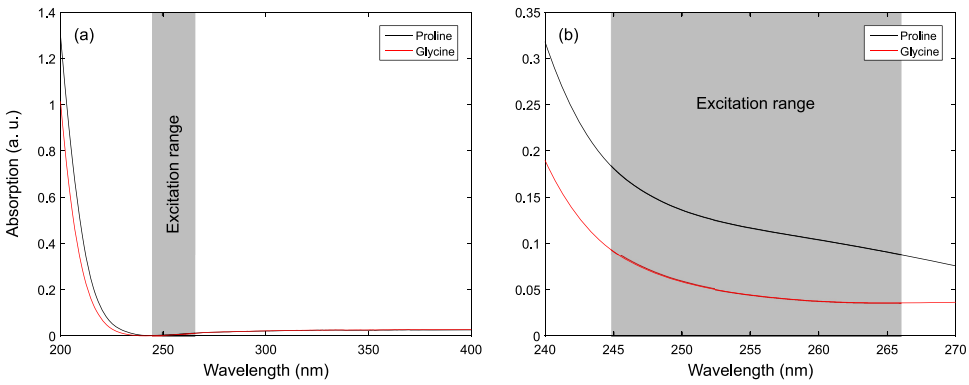

FIG. 3. Absorption spectra of the amino acids studied in this work. The excitation range used for RRS is indicated in gray. Panel (a) shows spectra of the two samples at concentrations chosen to ensure reliable absorption measurements by the spectrophotometer. The change in absorption within the Raman excitation range is indicated in (b) for samples with concentrations comparable to those used in the Raman experiments.

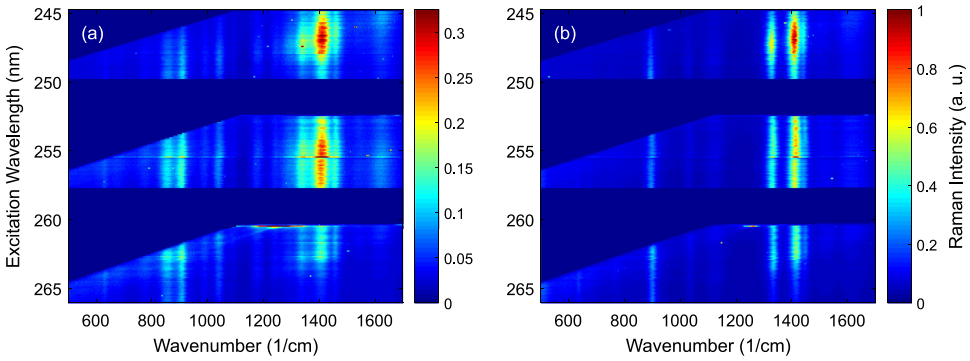

FIG. 5. Excitation-emission maps (EEM) of (a) proline and (b) glycine. Raman peaks appear as perpendicular lines. Optimal resonance conditions are marked by maximal Raman spectral amplitude.

measured via the photodiode during acquisition to compensate for power fluctuations of the laser. The measured Raman spectra processed that way constitute the EEM. All spectral features are shown at the correct positions, discounting possible grating inaccuracies. The data postprocessing procedure is very time-efficient (on the order of a few seconds for a full EEM) and ensures fast data processing even for large sets of Raman spectra and molecular species.

C. Resonance profiles

The final EEMs of proline and glycine are shown in Fig. 5. The maps are divided into three spectral regions according to the long pass filters used in the experimental setup. Note that more filter sets can be added to obtain full EEMs if required. According to the absorption spectra of proline and glycine (compare Fig. 3), a shorter excitation wavelength leads to an increase in the generated Raman intensity, showing the expected resonance enhancement in Raman scattering for the amino acids. The increase in absorption in the preresonant range is accompanied by an effectively larger Raman scattering cross section. In contrast to the absorption spectra, there is no continuous increase in the resonance profiles. This discrepancy is attributed to the finite accuracy in determining the DSRF. Nevertheless, a trend of increasing Raman intensity is obvious from Fig. 5, indicating the resonant enhancement in the Raman spectra.

IV. CONCLUSION

In this work, we have presented an experimental setup and a procedure for the acquisition of high-precision UV resonance profiles in Raman spectroscopy. The procedure includes an algorithm for data postprocessing enabling the investigation of any molecule at any wavelength. The setup is straightforward and the computational approach is fast and easy to implement. The concentrations of the samples used were selected according to the maximal solubility in water. For lower concentrations and Raman scattering cross sections, respectively, the applied energy and exposure time can be increased for recording of the resonance profiles.

The absorption spectra of the model species used, proline and glycine, suggest the preresonant increase of Raman scattering for shorter excitation wavelengths starting at approximately 260 nm. The EEMs reveal that shorter excitation wavelengths are more efficient for investigating the characteristic features of amino acids compared to longer wavelengths in the preresonant case. Choosing a shorter wavelength will increase the Raman intensity even further. Thus, when the excitation wavelength is shorter than 250 nm, the impact of fluorescence can faithfully be neglected. For molecules with a non-continuous increase of the absorption spectra in the preresonant range, the same qualitative behavior of the corresponding EEMs is expected. Samples exhibiting strong absorption in the excitation range need to be investigated via a setup operating in reflection mode. The experimental setup presented here can be modified accordingly. The procedure for data postprocessing is applied in the same manner. The application of a single light source for calibration and measurement prevents extensive modification of the experimental setup, thus sustaining the optical alignment and enabling a reliable calibration procedure for subsequent measurements. For identifying the optimal excitation wavelength to measure the Raman spectrum of a specific molecule, an accurate spectral calibration of the experimental setup is essential.

In general, in resonance Raman spectroscopy, the experimental setup is usually tailored to a certain group of molecules. The UV range used for investigating biomolecules such as proteins or amino acids requires a more complicated setup in terms of optics and coatings compared to the visible or near-infrared region in order to optimize the detection efficiency. The scattering cross section promotes the use of shorter excitation wavelengths, as a decrease by a factor of two in the wavelength increases the amount of scattered light by a factor of 16. Consequently, Raman spectroscopy in the UV benefits from the absorption of biomolecules in this range and the higher scattering cross section but has the disadvantage of lower detection efficiency as determined by the optical elements, the spectrometer, and the cameras used. On the other hand, Raman spectroscopy in the visible or near-infrared range benefits from a better detection efficiency but generally lacks the missing resonance enhancement.

On the basis of the procedure presented in this work, any experimental setup can be tailored to the specific needs of the analyte (e.g., optimal excitation wavelength).

ACKNOWLEDGMENTS

This work was supported by the DFG Cluster of Excellence EXC 1077/1 “Hearing4all.”

[1]D. Pratiwi, J. Fawcett, K. C. Gordon, and T. Rades, "Quantitative analysis of polymorphic mixtures of ranitidine hydrochloride by Raman spectroscopy and principal components analysis," Eur. J. Pharm. Biopharm. **54**, 337–341 (2002).
[2]A. L. Jenkins, R. A. Larsen, and T. B. Williams, "Characterization of amino acids using Raman spectroscopy," Spectrochim. Acta, Part A **61**, 1585–1594 (2005).
[3]E. Podstawka-Proniewicz, N. Piergies, D. Skołuba, P. Kafarski, Y. Kim, and L. M. Proniewicz, "Vibrational characterization of L-leucine phosphonate analogues: FT-IR, FT-Raman, and SERS spectroscopy studies and DFT calculations," J. Phys. Chem. A **115**, 11067–11078 (2011).
[4]Z. Chi, X. G. Chen, J. S. Holtz, and S. A. Asher, "UV resonance Raman-selective amide vibrational enhancement: Quantitative methodology for determining protein secondary structure," Biochemistry **37**, 2854–2864 (1998).
[5]S. Kecel, A. E. Ozel, S. Akyuz, S. Celik, and G. Agaeva, "Conformational analysis and vibrational spectroscopic investigation of L-proline–tyrosine (L-Pro–Tyr) dipeptide," J. Mol. Struct. **993**, 349–356 (2011).
[6]S. A. Oladepo, K. Xiong, Z. Hong, and S. A. Asher, "Elucidating peptide and protein structure and dynamics: UV resonance Raman spectroscopy," J. Phys. Chem. Lett. **2**, 334–344 (2011).
[7]E. Vass, M. Hollósi, F. Besson, and R. Buchet, "Vibrational spectroscopic detection of beta- and gamma-turns in synthetic and natural peptides and proteins," Chem. Rev. **103**, 1917–1954 (2003).
[8]A.-K. Kniggendorf, M. Meinhardt-Wollweber, X. Yuan, B. Roth, A. Seifert, N. Fertig, and C. Zeilinger, "Temperature-sensitive gating of hCx26: High-resolution Raman spectroscopy sheds light on conformational changes," Biomed. Opt. Express **5**, 2054–2065 (2014).
[9]R. Aroca, *Surface-Enhanced Vibrational Spectroscopy* (John Wiley & Sons, Ltd., Chichester, UK, 2006).
[10]S. A. Asher, "UV resonance Raman spectroscopy for analytical, physical, and biophysical chemistry," Anal. Chem. **65**, 59A–66A (1993).
[11]S. A. Asher, "UV resonance Raman spectroscopy for analytical, physical, and biophysical chemistry," Anal. Chem. **65**, 201A (1993).
[12]E. R. Holiday, "Spectrophotometry of proteins," Biochem. J. **30**, 1795–1803 (1936).
[13]K. Imahori and J. Tanaka, "Ultraviolet absorption spectra of poly-L-glutamic acid," J. Mol. Biol. **1**, 359–364 (1959).
[14]X. Zhao, R. Chen, C. Tengroth, and T. G. Spiro, "Solid-state tunable kHz ultraviolet laser for Raman applications," Appl. Spectrosc. **53**, 1200–1205 (1999).
[15]S. J. Doig and F. G. Prendergast, "Continuously tuneable, quasi-continuous-wave source for ultraviolet resonance Raman spectroscopy," Appl. Spectrosc. **49**, 247–252 (1995).
[16]F. Inagaki, M. Tasumi, and T. Miyazawa, "Excitation profile of the resonance Raman effect of β-carotene," J. Mol. Spectrosc. **50**, 286–303 (1974).
[17]S. A. Asher, R. W. Bormett, X. G. Chen, D. H. Lemmon, N. Cho, P. Peterson, M. Arrigoni, L. Spinelli, and J. Cannon, "UV resonance Raman spectroscopy using a new cw laser source: Convenience and experimental simplicity," Appl. Spectrosc. **47**, 628–633 (1993).
[18]R. L. Benson, K. Iwata, W. L. Weaver, and T. L. Gustafson, "Improvements in the generation of quasi-continuous, tunable ultraviolet excitation for Raman spectroscopy: Applications to drug/nucleotide interactions," Appl. Spectrosc. **46**, 240–245 (1992).
[19]F. Rwere, P. J. Mak, and J. R. Kincaid, "Resonance Raman determination of vinyl group disposition in different derivatives of native myoglobin and its heme-disoriented form," J. Raman Spectrosc. **45**, 97–104 (2014).
[20]X. Zhao and T. G. Spiro, "Ultraviolet resonance Raman spectroscopy of hemoglobin with 200 and 212 nm excitation: H-bonds of tyrosines and prolines," J. Raman Spectrosc. **29**, 49–55 (1998).
[21]L. D. Ziegler, "Resonance Raman scattering of benzene and benzene-d_6 with 212.8 nm excitation," J. Chem. Phys. **74**, 982 (1981).
[22]B. Sharma, S. V. Bykov, and S. A. Asher, "UV resonance Raman investigation of electronic transitions in α-helical and polyproline II-like conformations," J. Phys. Chem. B **112**, 11762–11769 (2008).
[23]B. Sharma and S. A. Asher, "UV resonance Raman investigation of the conformations and lowest energy allowed electronic excited states of tri- and tetraalanine: Charge transfer transitions," J. Phys. Chem. B **114**, 6661–6668 (2010).
[24]B. Sharma and S. A. Asher, "UV resonance Raman finds peptide bond-Arg side chain electronic interactions," J. Phys. Chem. B **115**, 5659–5664 (2011).
[25]D. R. Lide, *Handbook of Chemistry and Physics* (CRC Press, Boca Raton, FL, 2005).
[26]C. R. Johnson, M. Ludwig, and S. A. Asher, "Ultraviolet resonance Raman characterization of photochemical transients of phenol, tyrosine, and tryptophan," J. Am. Chem. Soc. **108**, 905–912 (1986).
[27]S. A. Asher and C. R. Johnson, "Raman spectroscopy of a coal liquid shows that fluorescence interference is minimized with ultraviolet excitation," Science **225**, 311–313 (1984).
[28]M. Koch, C. Suhr, B. Roth, and M. Meinhardt-Wollweber, "Iterative morphological and mollifier-based baseline correction for Raman spectra," J. Raman Spectrosc. **48**, 336 (2017).